We are IntechOpen, the world's leading publisher of Open Access books Built by scientists, for scientists

6,900
Open access books available

185,000
International authors and editors

200M
Downloads

Our authors are among the

154
Countries delivered to

TOP 1%
most cited scientists

12.2%
Contributors from top 500 universities



WEB OF SCIENCE™

Selection of our books indexed in the Book Citation Index in Web of Science™ Core Collection (BKCI)

Interested in publishing with us?
Contact book.department@intechopen.com

Numbers displayed above are based on latest data collected.
For more information visit www.intechopen.com



Chapter 1

The Solutions of DC-DC Converters for Renewable Energy System

Nguyen The Vinh and Vo Thanh Vinh

Additional information is available at the end of the chapter

http://dx.doi.org/10.5772/intechopen.78768

Abstract

Photovoltaic and wind systems have been used for a few years to bring a new power supply to many applications, while preserving the environment. This chapter is interested in this work at low and medium power, a few 100 W, for applications to housing and buildings. The works consider a system in which the various sources of renewable energies are connected to each other in a parallel structure which supposes the use of specialized converters accepting at the input voltages of the order of a few tens of volts, and giving out several hundred of volts. The DC-DC converters with magnetic coupling will be analyzed more particularly to show the technological limits. In particular, the influence of the magnetic circuit and the leakage flows will be studied in more detail.

Keywords: renewable energy systems, DC-DC converter, voltage step-up, coupled conductor

1. Introduction

Optimizing the use of renewable sources for the production of electrical energy is one of the possible answers that can be useful for saving exhaustible fossil energy resources. Nevertheless, the use of renewable energies induces the development of new utilities and even architectures and systems. The management and optimization of the conversion and distribution of electrical energy produced from several different renewable energy sources is a challenge for stable, sustainable energy production systems that are isolated, autonomous and stable. The choice of a high-voltage direct current bus (HVDC bus) for the distribution of energy in the energy production chain can be considered as part of an efficiency improvement strategy [1–3]. The HVDC bus has the advantage of using smaller cross sections of cables than those traditionally

IntechOpen

© 2018 The Author(s). Licensee IntechOpen. This chapter is distributed under the terms of the Creative Commons Attribution License (http://creativecommons.org/licenses/by/3.0), which permits unrestricted use, distribution, and reproduction in any medium, provided the original work is properly cited. CC BY

used in AC networks, allowing a reduction in the costs of transport and distribution of electricity. In addition, the HVDC bus is more secure against any fraud of diversion of the produced electricity and provides a global distribution with more security. The distributed, autonomous or interconnected production units corresponding to the energy production systems considered here are generally characterized by a large input current and a low input voltage associated with a high output voltage. This HVDC bus architecture imposes a two-wire topology for the power conversion system connected to an AC distribution network. In this architecture, the distributed power is connected to an alternating current network by means of an intermediate HVDC bus. The DC-DC converters with a basic voltage ratio are integrated upstream, just behind the supply of the energy source or sensors (for example as photovoltaic panels).

Downstream of the HVDC bus is near power generation, a DC-AC inverter is inserted at the interface to convert the HVDC to standard AC, typically according to country specific standardization, 110, 220 or 380 V. In this solution, for optimum conversion efficiency, software drives the system assuming that tracking of the source's maximum power point is directly implemented in the controller of each of the individual DC-DC converters. Thus, as seen in a renewable energy production chain, the individual DC-DC converter integrated into the power generator is one of the most important electronic elements. This converter must take into account a set of characteristics and technological constraints related to the power delivered by the source, whether photovoltaic or other as:

The converter must be able to convert the energy to a range of input voltages between 12 and 60 V which is the upper limit of the no-load voltage for a panel of 60 cells, knowing that in the load the MPP is around 30 V.

The output voltage provided by the converter must be able to reach 240VDC which represents the limit set for this first converter version. An upcoming version should be proposed to have a voltage output of 400 VDC and several kV.

The power to be converted must be greater than 150 W, corresponding to the panels available in the laboratory.

The performance wished is 98%. This value is obviously an average limit, as inverter manufacturers advertise the performance of their devices for an optimal operating point.

The converter must be remotely controlled via a fieldbus.

It must be able to stop production in the event of a fault or a special order for the safety of the installation or for maintenance.

Of all the constraints, it is possible to select three main that motivate our work and are causing numerous research worldwide, that is to say, excellent performance, high voltage gain and a small volume. Other constraints are added such as thermal, mechanical, but have not been taken into account in this work which is mainly focused on the electronic properties of the converter [4]. It should be noted that the aforementioned constraints related to the integration of DC-DC converters in grid-connected electrical generators are specific to the power supply system for power from sources energy renewable.

http://dx.doi.org/10.5772/intechopen.78768

Nevertheless, most industrial applications require efficient DC-DC converters. As examples, we can note the high intensity discharge ballasts for lamps used in automobile or the front converter with two inputs (a main AC [AC] network and a battery to support DC power supplies) to replace the common but complex emergency power supplies (UPS-uninterruptible power supply) in the computer and telecommunications industries [5]. Nevertheless, for a system of electricity generation from photovoltaic energy or another individual source, due to the variable nature of the input power of the converter, and the almost constant high voltage output hundred a set of additional features specific, necessary and are presented below.

Many works in the literature present these systems and we quote some important references [6]. In order to overcome the drawbacks of basic converters which prove to be unsuitable for photovoltaic energy production systems, as we have pointed out above, various authors, taking into account the different specific constraints of this demand, present an investigation on the many topologies of possible converters [7]. The solution considered simplest is composed of several converters in cascade to obtain the desired gain [8]. Even if we do not take into account synchronization problems inherent to active switches, this solution is not optimal from an economic point of view and the losses by the multiplication of the components and the overall efficiency of the converter low due to the number important components. In addition, this solution does not meet the constraint of reduced size.

The solution considered, which will be described below, is to adjust the high voltage gain (Step-Up), by choosing a suitable ratio of turns of a transformer or inductance coupled to an independent converter [9]. Comparing with a base of transformer converters, a coupled inductance converter in its basic configuration requires few components. Due to its less complicated structure and the smaller, larger ripple of the primary winding current, it requires filtering of input capacitance. This results in lower current stress and more conduction losses low. The converters based on the coupled inductors technique allow the adjustment of the requested voltage with respect to the input voltage by a judicious choice of the transformation ratio m between the coils, which makes it possible to keep a cyclic ratio very near to 1/2, thus guaranteeing an excellent internal energy transfer rate. Unfortunately, an increase in m results in an increase in the trapped energy in the leakage inductances, and even for the low transformation ratios, the result is a degradation of the efficiency. In this converter topology, and in order to achieve a high Step-Up gain, some authors propose efficient solutions resulting in modified topologies obtained by increasing the complexity of the basic version in **Figure 1** [10, 11].

In analyzing the performance of coupled-coupled transformers or converters, authors generally consider the coupling factor of windings to be a fixed value, theoretically equal to one. It follows from the nonpractical validity of this hypothesis that in order to make DC-DC converters effective, the current approach is often chosen, once again, to correct the defects by adding modifications to the basic topology and adding electronic components of various protections [12]. In converters based on the transformer of Forward and the push-pull as described [13–15], the transformer produces a lot of losses and the switches of these converters suffer from high voltage spikes and high power dissipation caused by the leakage inductances, and important currents.

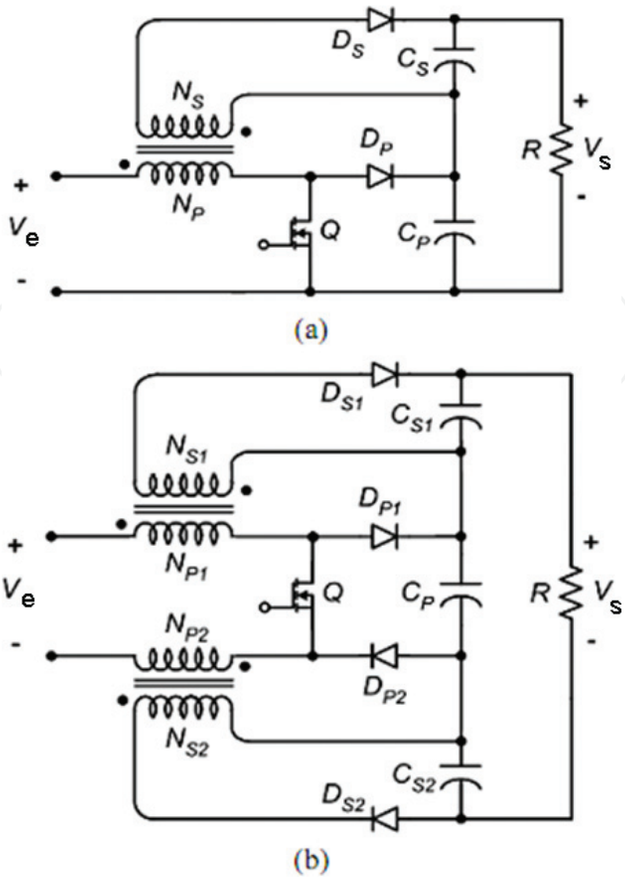


Figure 1. Unbalanced and balanced switching converter. (a) Converter balanced of conventional, (b) converter of equilibrium.

To avoid these disadvantages, some authors suggest the introduction of passive elements that diode and capacitor which gives rise to many variants of Boost, Buck-Boost, with as a direct consequence an increase in the cost due to a switch supplement of power, volume and complexity [16]. For this reason and for all the aforementioned drawbacks of converter topologies, for PV generator applications, coupled inductance converters are practical, even for transformer-based converters, to reach the high voltage ratio and conserve a small volume. With this approach, we complete the efficiency analysis proposed in this chapter and follow up on our previous study of losse on the swith in the process on–off in the converter dedicated to converting energy from photovoltaic sources. Analysis of the influence of leak inductances in the magnetic circuit for direct magnetic coupling and limiting energy leakage by circuit recovery in the DC-DC converter.

2. Analysis and calculation of leakage inductances

This type of calculation is difficult to carry out accurately, and only the finite element codes are able to give an accurate result. In the vast majority of cases, however, such precision is not useful and one can be content with an order of magnitude and sometimes even simply with a

http://dx.doi.org/10.5772/intechopen.78768

sense of variation. For a transformer used with ETD ferrite core, where the best possible result is sought, the finalization of a transformer can hardly be done until after experimentation, rendering a "precise" calculation unattractive. It will place ourselves voluntarily in an elementary case, with the load to the reader to adapt it according to his needs. The configuration of this work will be that of two concentric circular windings [17–19].

The principle of calculating the leakage inductances in a magnetic component comprising a core can be explained from the section of **Figure 2**, corresponding to a transformer with two concentric windings wound on the central core of a magnetic circuit with three branches and separated by a layer of insulation.

In the hypothesis of a zero magnetizing current, the sum of the ampere-turns present in the coils is zero. But if we choose any closed contour passing through the window, it immediately appears that the application of Ampère's theorem highlights the existence of a nonzero magnetic module excitation vector H. We can deduce that there is an electromagnetic energy stored in the window through the relation:

$$W_{EM} = \iiint \frac{\mu_0 . H^2}{2} . dV \tag{1}$$

This energy corresponds by definition to field lines which do not enclose the entirety of the two coils. It is actually a leak energy to which we can associate a leakage inductance. Volume *"V"* of magnetic component we have shown that the product of the areas characterized the magnetic component.

Whatever the form of the component, it is necessary to retain the following first approximations:

The system is observed by freezing the currents (modules I_1 and I_2) in the coils.

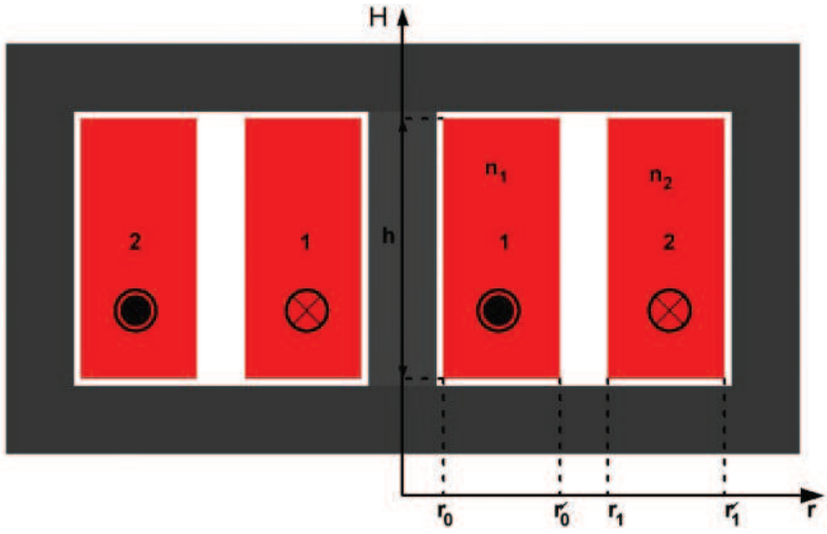


Figure 2. Cutting of a magnetic component for the calculation of leakage inductances.

The modulus H of the magnetic excitation is null (negligible) in the nucleus and, as a corollary, the magnetizing current is zero.

The field lines in the window are perfectly rectilinear and orthogonal to the direction of progression of the ampere-turns, noted overall *N. I*.

Ampere-turns are homogeneously distributed, continuous and unobtrusive in the section of the windings.

Case of concentric windings: According to these hypotheses, in the diagram of **Figure 3**. The two coils will have the same height h (the dimension of a height and the name of the average height of the field lines: this quantity is available for a given kernel in the manufacturer's documentation), start and end rays respectively H depends only on r and is written:

$$H(r) = \frac{N.I}{h} \tag{2}$$

This form results from the application of the Ampère theorem, by choosing a closed contour, of any form in the nucleus since H is zero, and closing in the window in the direction of the field lines. At the same time, we can represent, again in the case of **Figure 3**, the progression of *N.I* and H as a function of *r*:

The progression of H in the window has the same form, taking into account the expression of H(r) and the maximum value reached which is here *N1.I1 = N2.I2*.

The next problem is that of volume integration. It is clear that if the component does not show a rough symmetry of revolution, H will become a two-dimensional or even three-dimensional function, out of the context of a given section of the component. The calculation is imaginable, but would lead to totally unworkable analytical expressions. We are therefore forced to limit ourselves to magnetic structures presenting a quasi-symmetry of revolution. The so-called potted nuclei correspond relatively well to this hypothesis.

It should be noted that the principles of calculation presented here are often used in cases where there is a clear absence of any form of symmetry of revolution (structure in E for example). If it seems that the application of the described method gives, in these latter cases,

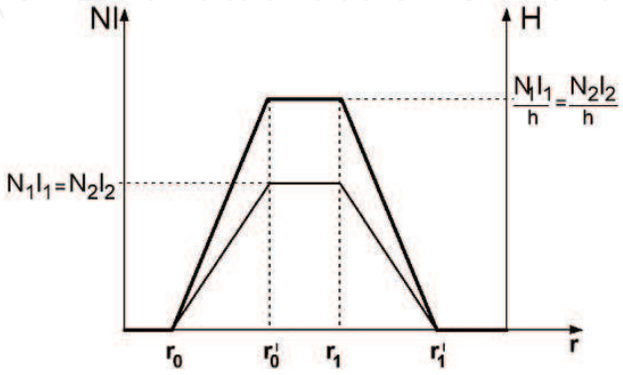


Figure 3. Progression of ampere-turns and H(r) in the window.

relatively correct results, the readers must be warned of the high level of approximation which this assumes and which is justified only by experience. Caution is therefore required [18, 19].

If we return to the hypothesis of the symmetry of revolution evoked above and always within the framework of our example, we can then express W_{EM} in the form:

$$W_{EM} = \int_{r_0}^{r'_1} \frac{\mu_0 . H^2(r)}{2} . 2\pi . h . r . dr \tag{3}$$

As mentioned above, it can be identified with the energy stored in an overall leakage inductance defined, as desired, with respect to the primary or secondary winding.

$$W_{EM} = \int_{r_0}^{r'_1} \frac{\mu_0 . H^2(r)}{2} . 2\pi . h . r . dr = \frac{1}{2} l_{f12} . I_1^2 = \frac{1}{2} l_{f21} . I_2^2 \tag{4}$$

In the concentric windings structures, on each interval of the window, H is always proportional to N1.I1 or N2.I2, depending on the chosen option. In the example of **Figure 4**, the H expressions are:

$$\text{To} \begin{cases} r_0 \le r \le r'_0 & H = \dfrac{N_1 . I_1 . (r'_0 - r)}{h(r'_0 - r_0)} = \dfrac{N_2 . I_2 . (r'_0 - r)}{h(r'_0 - r_0)} \\ r'_0 \le r \le r_1 & H = \dfrac{N_1 . I_1}{h} = \dfrac{N_2 . I_2}{h} \\ r_1 \le r \le r'_1 & H = \dfrac{N_1 . I_1 . (r'_1 - r)}{h(r'_1 - r_1)} = \dfrac{N_2 . I_2 . (r'_1 - r)}{h(r'_1 - r_1)} \end{cases} \tag{5}$$

We will then end up with general relations of the form:

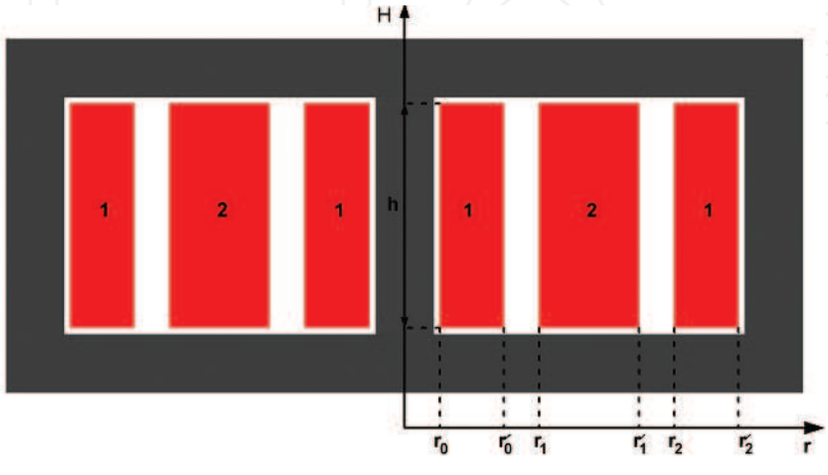


Figure 4. Types with nested concentric windings.

$$\frac{1}{2} l_{f12} . I_1^2 = \pi . \mu_0 \frac{(N_1 . I_1)^2}{h} \int_{r_0}^{r'_1} X^2(r) . rdr \tag{6}$$

$$\frac{1}{2} l_{f21} . I_2^2 = \pi . \mu_0 \frac{(N_2 . I_2)^2}{h} \int_{r_0}^{r'_1} X^2(r) . rdr \tag{7}$$

$$\text{with } X(r) = \frac{h.H(r)}{N_1 . I_1} = \frac{h.H(r)}{N_2 . I_2} \tag{8}$$

piecewise affine function from which we deduce:

$$l_{f12} = 2\pi . \mu_0 \frac{N_1^2}{h} \int_{r_0}^{r'_1} X^2(r) . rdr \tag{9}$$

$$l_{f21} = 2\pi . \mu_0 \frac{N_2^2}{h} \int_{r_0}^{r'_1} X^2(r) . rdr \tag{10}$$

At this level, one gets expressions that remain relatively heavy. A last approximation is possible if the thickness of each winding is small in front of its mean radius. We can then identify the surface element 2 μ.rdr at 2 μ.rBdr, where rB is the average radius of the considered winding (equivalent to an approximate integration by the method of the rectangles).

In the example studied, we obtain the following expression (case of l_{f12}):

$$l_{f12} = 2\pi . \mu_0 \frac{N_1^2}{h} \left[\frac{r_0 + r'_0}{2} \int_{r_0}^{r'_0} X^2(r) dr + \frac{r'_0 + r_1}{2} \int_{r'_0}^{r_1} X^2(r) dr + \frac{r_1 + r'_1}{2} \int_{r_1}^{r'_1} X^2(r) dr \right] \tag{11}$$

$$\text{with } \begin{cases} X(r) = \dfrac{r'_0 - r}{r'_0 - r_0} & \textit{for the first fiddling} \\ X(r) = 1 & \textit{for insulation} \\ X(r) = \dfrac{r'_1 - r}{r'_1 - r_1} & \textit{for the second fiddling} \end{cases} \tag{12}$$

The final result will be:

$$l_{f12} = \pi . \mu_0 . N_1^2 \frac{r'_1 2 + 2r_1^2 - 2r'_0 2 - r_0^2}{3h} \tag{13}$$

Case of l_{f21}:

$$l_{f21} = \pi.\mu_0.N_2^2 \frac{r_1'2 + 2r_1^2 - 2r_0'2 - r_0^2}{3h} \tag{14}$$

It would be really interesting to compare the theory with the case which concerns us concretely to see above.

In this instance concentric coils nested **Figure 5**, the method is the same as for the analysis of concentric windings. The final result will be:

$$l_{f12} = \pi.\mu_0.N_1^2 \frac{2\left(r_1^2 + r_2^2 - r_0'2 - r_1'2\right) + r_2'2 - r_0^2}{12h} \tag{15}$$

This simplification can be extended to any number of winding elements. In the case of the parameters of the first and second coils, they are in fluence leakage inductance.

In the case of concentric windings nested with the four-part primary winding division, **Figure 5**:

$$\begin{aligned} l_{f12} = 2\pi.\mu_0 \frac{N_1^2}{h} \Bigg\{ & \frac{r_0 + r_0'}{2} \int_{r_0}^{r_0'} X^2(r)dr + \frac{r_0' + r_1}{2} \int_{r_0'}^{r_1} X^2(r)dr + \\ & + \frac{r_1 + r_1'}{2} \int_{r_1}^{r_1'} X^2(r)dr + \frac{r_2 + r_1'}{2} \int_{r_1'}^{r_2} X^2(r)dr + \\ & + \frac{r_2' + r_2}{2} \int_{r_2}^{r_2'} X^2(r)dr + \frac{r_3 + r_2'}{2} \int_{r_2'}^{r_3} X^2(r)dr + \\ & + \frac{r_3 + r_3'}{2} \int_{r_3}^{r_3'} X^2(r)dr + \frac{r_3' + r_4}{2} \int_{r_3'}^{r_4} X^2(r)dr + \frac{r_4 + r_4'}{2} \int_{r_4}^{r_4'} X^2(r)dr \Bigg\} \end{aligned} \tag{16}$$

$$l_{f12} = \pi.\mu_0.N_1^2 \frac{2\left(r_1^2 + r_2^2 + r_3^3 + r_4^2 - r_0'2 - r_1'2 - r_2'2 - r_3'2\right) + r_4'2 - r_0^2}{24h} \tag{17}$$

Case of superimposed windings: The physical model of this structure is obtained in the same way as previously. The flow model inside the core and the windings is derived using Ampere's law and the integration show path in **Figure 6a**. Field strength through the core and windings is shown in **Figure 6b**. The sign of the intensity of the field determines the direction flows inside the core and the windings. This at its turn determines the flow pattern within the structure which is illustrated in **Figure 6b**.

In the case of superimposed components (**Figure 6a**), the method is identical, but the assumptions are different. The leakage inductances can be estimated and the calculation of the amount of energy stored in each of the winding can be done by shorting the secondary "mathematically."

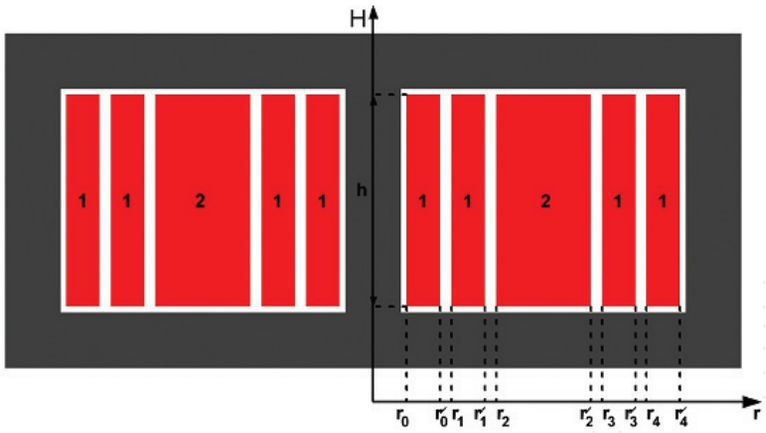


Figure 5. Types with nested concentric windings (winding primary four part).

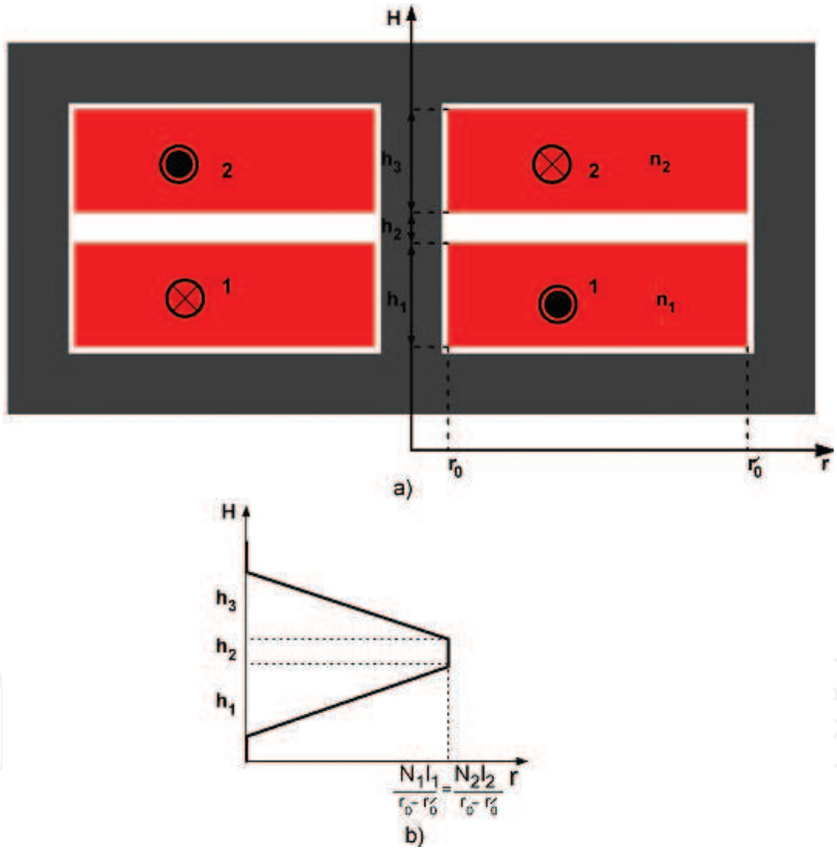


Figure 6. Case of superimposed windings.

The field strength with the short-circuited secondary is similar to that of **Figure 6b**, with the mutual flow reduced to about 0.

Compared to the previous case, the progression of Ampere-turns is done according to the vertical axis. H now depends only on h. The expression of W_{EM} becomes:

$$W_{EM} = \int_0^{hT} \frac{\mu_0 . H^2(h)}{2} . \pi \left(r_0' 2 - r_0^2 \right) . dh \tag{18}$$

We obtain:

$$W_{EM} = \int_0^{hT} \frac{\mu_0 . H^2(h)}{2} . \pi \left(r_0' 2 - r_0^2 \right) . dh = \frac{1}{2} . l_{f12} . I_1^2 = \frac{1}{2} . l_{f21} . I_2^2 \tag{19}$$

The calculation is then quite similar to the previous one, initially expressing H(h) on the different zones.

In the concentric windings structures, on each interval of the window, H is always proportional to *N1I1* or *N2I2*, depending on the chosen option. In the example of **Figure 6b**, the expressions of H are:

$$\begin{cases} height\ \mathrm{h}_1 \quad H = \dfrac{N_1 . I_1 . h}{h_1 \left(r_0' - r_0 \right)} = \dfrac{N_2 . I_2 . h}{h_1 \left(r_0' - r_0 \right)} \\ height\ \mathrm{h}_2 \quad H = \dfrac{N_1 . I_1}{\left(r_0' - r_0 \right)} = \dfrac{N_2 . I_2}{\left(r_0' - r_0 \right)} \\ height\ \mathrm{h}_3 \quad H = \dfrac{N_1 . I_1 . h}{h_3 \left(r_0' - r_0 \right)} = \dfrac{N_2 . I_2 . h}{h_3 \left(r_0' - r_0 \right)} \end{cases} \tag{20}$$

In the example studied, we obtain the following expression (case of l_{f12}):

$$l_{f12} = \pi . \mu_0 . \frac{N_1^2}{\left(r_0' - r_0 \right)^2} \left\{ \int_0^{h_1} H^2(h) . \left(r_0' 2 - r_0^2 \right) . dh + \int_0^{h_2} H^2(h) . \left(r_0' 2 - r_0^2 \right) . dh + \int_0^{h_3} H^2(h) . \left(r_0' 2 - r_0^2 \right) . dh \right\} \tag{21}$$

The final result will be:

$$l_{f12} = \pi . \mu_0 . N_1^2 . \frac{\left(r_0' + r_0 \right) \left(h_1 + 3h_2 + h_3 \right)}{3 \left(r_0' - r_0 \right)} \tag{22}$$

This type of calculation, be it overlapping concentric overlapping or overlapping structures, presents no particular difficulty but is not extremely light. We give the result for four typical two-part superimposed overlapping windings with two-part primary winding division in **Figure 6**, and superimposed overlapping windings with four-part primary winding splitting. The method of analysis is the same as that of concentric windings. The final result will be:

$$l_{f12} = \pi . \mu_0 . N_1^2 . \frac{\left(r_0' + r_0 \right) \left(h_1 + 3h_2 + h_3 + 3h_4 + h_5 \right)}{12 \left(r_0' - r_0 \right)} \tag{23}$$

In the case of nested concentric windings with four-part primary winding division:

$$l_{f12} = \pi.\mu_0.N_1^2.\frac{(r'_0 + r_0)(h_1 + 3h_2 + h_3 + 3h_4 + h_5 + 3h_6 + h_7 + 3h_8 + h_9)}{24(r'_0 - r_0)} \tag{24}$$

The final comparison with the theoretical calculations will follow to confirm the veracity of the theoretical approach with the experience of measurement.

In order to accurately predict the behavior of the converter, a preliminary measurement of the transformer coupling coefficient is necessary. The method used to determine the inductance of the two inductance coils consists of two sequential measurements on the basis of taking into account the additive and subtractive contribution of the magnetic flux of the inductor windings connected in series. So, we obtained two inductor values, named respectively L12M and L12m defined by

$$L_{12M} = L_1 + L_2 + 2M \tag{25}$$

$$L_{12m} = L_1 + L_2 \tag{26}$$

With:

L_{12M}: the measurement of the series inductance with the opposite direction windings.

L_{12m}: the series measurement with the same direction windings.

Thus, it is possible to deduce the value of M representing the coupling inductance

$$M = \frac{L_{12M} - L_{12m}}{4} \tag{27}$$

In carrying out our experiments $L_{12M} = 168mH$ and $L_{12m} = 75mH$. So, we deduce the value of M = 23.25 mH representing a coupling factor k given by the classical formula:

$$k = \frac{M}{\sqrt{L_1.L_2}} = 0,981 \tag{28}$$

This high value of k corresponds to a transformer quality and allows a good performance of the converter.

According to magnetic circuit EDT54 in the transformer (the inductance $L_1 = 31.6mH$ measured; $N_1 = 32spires$) and Eq. (24) we gave factor k calculated such that:

$$l_{f12-calculate} = 0,812mH$$

$$k_{caculate} \simeq 0.987$$

It is easy to see that the total leakage inductance brought back to the primary is reduced in the concentric coils and superimposed coils. This technique is one that is commonly used in energy conversion in DC-DC converters to reduce the leakage inductance and thus extend the

bandwidth to high frequencies. In practice, we will meet from two to four interlacing, larger numbers posing major problems of realization. It is of course also possible to reduce the leakage inductance by decreasing the number of turns of the windings, which is possible if the permeability of the core is increased. This generally requires the use of nickel alloys, permalloys and derivatives or mumetal. The extra cost generated by these materials makes it possible to justify this technique only for link transformers and for realizations the cost price of which does not count for very little. Still for the link transformers, and in some output transformers, it is possible to use multi-wire windings wound together, which further improve the primary-secondary coupling but having the defect of a low electrical isolation. Very careful achievements can achieve a high cut of (30–100) kHz.

3. Solution for DC-DC Flyback converter

3.1. Flyback converter with nonlinear magnetic coupling

When the switch is conducting, the energy is stored in the primary inductance as well as in the corresponding leakage inductance. The leakage flux associated with the leakage inductance of the primary winding is not transferred to the secondary winding, and it is therefore necessary to manage the energy associated with this leakage flow either by dissipating it in an external circuit (known as damping), or by recycling it. Unless this energy finds a path, it will occur at a peak voltage across the windings that could destroy the switching circuit (see **Figure 7**). The greater the leakage inductance of all transformer isolated DC-DC converters can lead to ring, an increase in voltage constraints, and an increase in power loss, resulting in a significant degradation of the performance of the circuit.

Figure 7 shows a practical Flyback converter modeled. The solution for the recovery circuit consists of a fast recovering series diode in the output winding with a combination of a

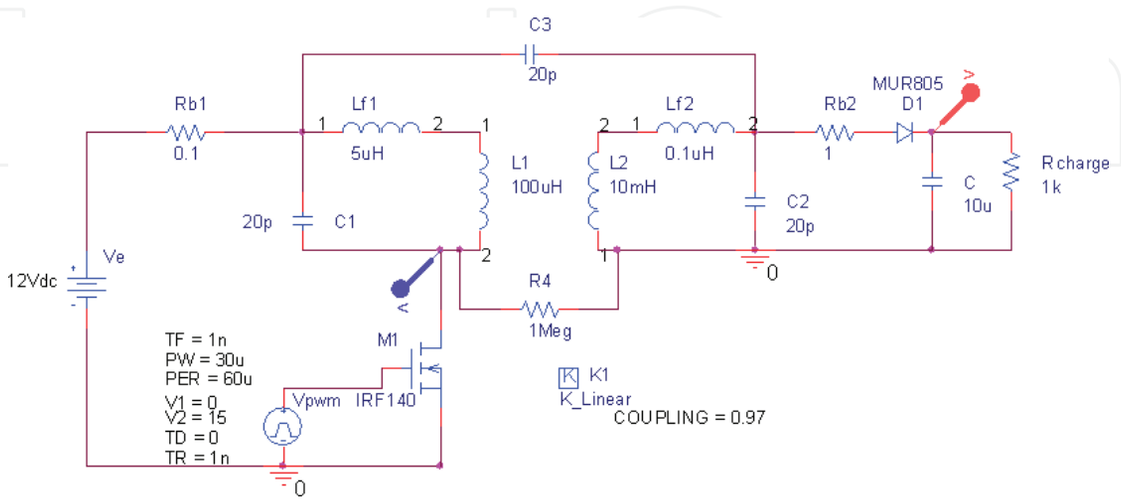


Figure 7. Basic diagram of a Flyback converter with leakage inductance in the transformer.

damping capacitor and a parallel resistor [13, 20] making load for the simulation. The current of the primary winding of leakage inductance has a low impedance path during the conduction of M1. It can be seen that at the end of the conduction of the diode D1, the voltage across the output filter capacitor will be at the higher potential. To check for excessive build-up voltage across the damping capacitor a resistor is placed across. According to the equilibrium state of this resistor is intended to dissipate the leakage flux energy.

The waveforms described above are only valid if all components are considered perfect. In fact, one can observe an overvoltage when opening the transistor operating as a controlled switch. This overvoltage comes from the energy stored in the leakage inductance Lf at the primary of the transformer. The energy it contains at the time of opening of the transistor cannot be transferred to the secondary. The evacuation of the energy stored in this parasitic inductance will be transferred to the parasitic capacitances of the transistor and the primary of the transformer by creating an overvoltage at the terminals of the transistor. As the primary has an inductive impedance, the cancelation of the current passing through the switch cannot be done under a zero voltage, so it will generate switching losses The effects damaging these overvoltages are detrimental to the transistor and therefore require the addition of switching assistance circuits. There is also secondary leakage inductance. This inductance will also cause losses and decrease the energy supplied by the power supply to the load. In the case of power supply having multiple outputs, secondary leakage inductances will create different losses on each of the outputs.

In this case, however, the locking of the switch interrupts the current through the leakage inductance of the transformer, and this will produce a voltage spike on the drain of MOSFET. The inductance will then resonate with the parasitic capacitances of the circuit, producing a high frequency high frequency wave as shown in **Figures 8** and **9**. On the Flyback primary, the measured leakage inductance resonates with the primary capacitances.

Many application and design notes ignore the resonance and make the converter work without addressing the issue. There are two problems related to resonance phenomena: first, the voltage, when excessive on the MOSFET drain, can cause the entail breaking of the transistor, and finally the failure of the device. Secondly, the resonance energy will be radiated and

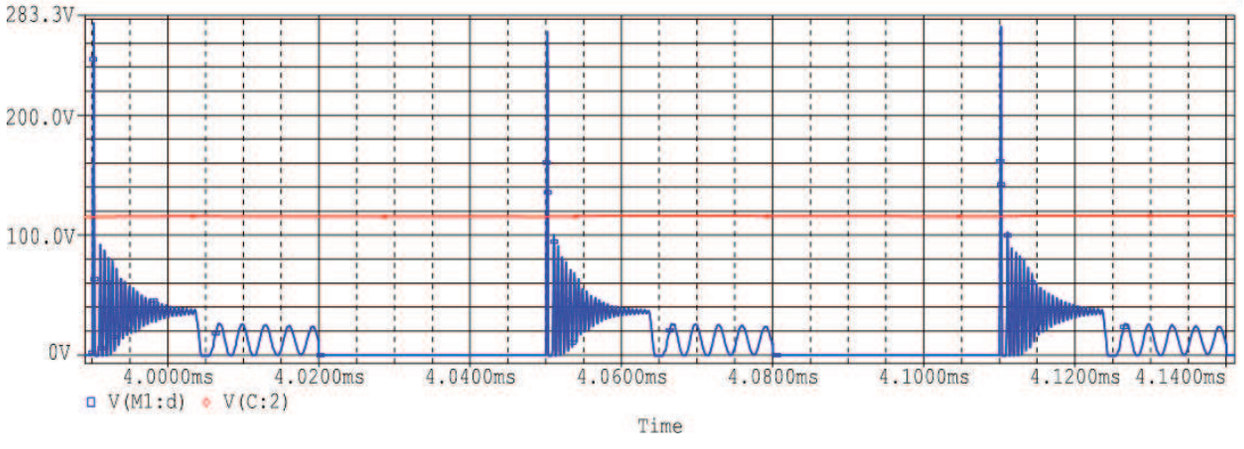


Figure 8. Simulation of the voltages obtained on a fly-back with a non-ideal transformer. The output voltage remains close to that on the transistor.

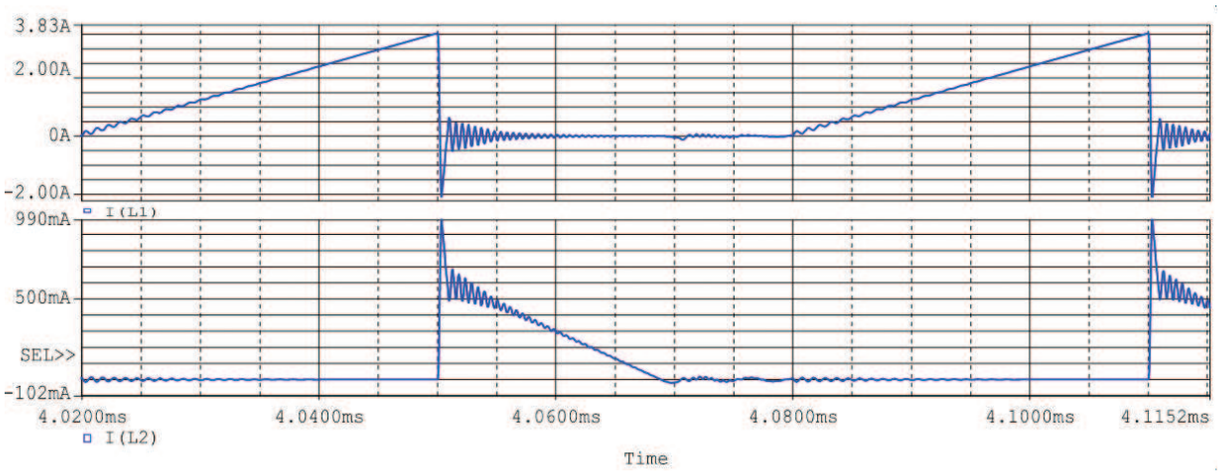


Figure 9. The current passed primary and secondary transformer inductance obtained modeling modeled with leakage inductance.

conducted everywhere in the power supply, load, and electronic control system, which creates noise problems and even random errors or failures in the logic part. Therefore, the frequency of the resonance will appear as a peak in the IEM spectrum and will be propagated in both "radiated" and "led" modes.

3.2. Flyback converter with recovery stage

Figure 10 shows the Flyback converter with the recovery stage (F-RS converter), the F-RS converter scheme in **Figure 10** shows the two main active inductors, L8, L9 and the two additional leakage inductors, constituted by a diode D5 in series, and a capacitor in parallel,

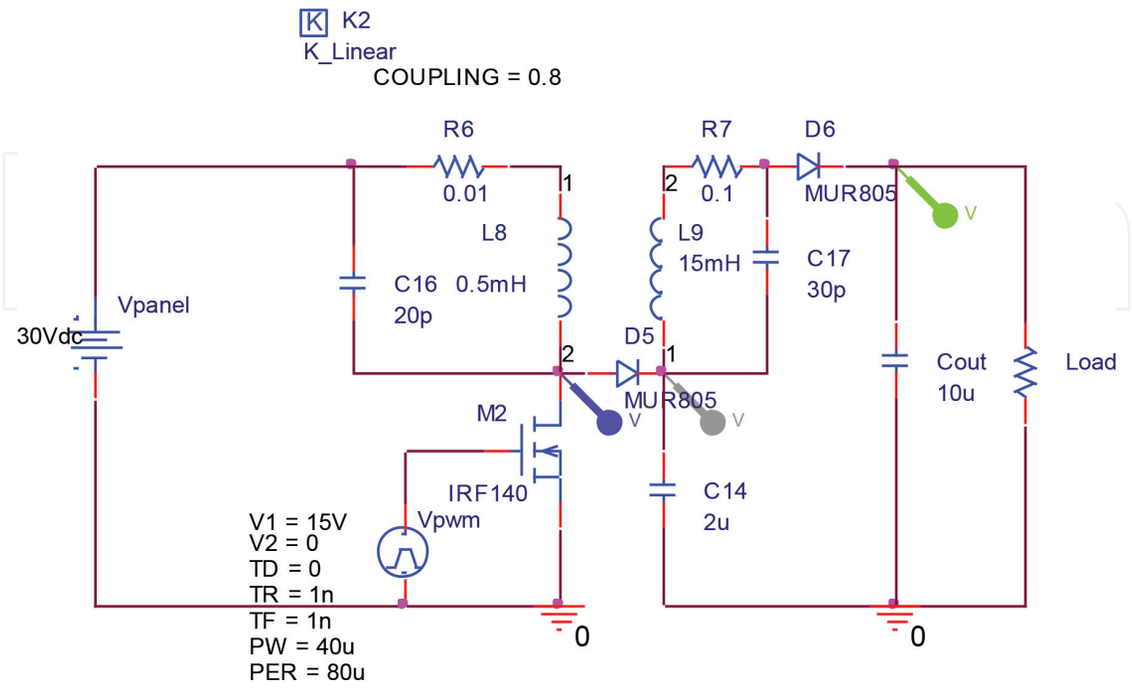


Figure 10. Model diagram for the simulation of the F-RS converter.

inserted between the two coupled inductance coils. Finally, the principle of the F-RS converter is based on an Flyback converter, voltage step-up base arrangement as described above, a recovery stage, and a second output amplifier stage. This recovery step should recover all normally lost energies in the standard basic MCB structure. This recovery step should recover all normally lost energies in the standard basic Flyback structure. In fact, even if the energy lost in the leakage inductances is only a small but significant percentage of the total transferred energy, this energy must be recycled during the shutdown time when there is an increase in efficiency overall conversion.

In this converter principle, the capacitor C is charged by the recovery energy initially stored in the leakage inductance coil L8 via the diode D5. It remains to ensure that the recovered leakage energy stored in the first pulse is not too large to cause a local increase of the voltage V_{C14}, which limits the voltage across the switch, Vds below an acceptable value.

We performed simulations of the MCB-RS converter under OrCad software. Magnetic coupling was deliberately chosen at a low value (k = 0.8) for the purpose of highlighting the effect of magnetic leakage. The transformation ratio was chosen as m = 20 in accordance with the prototype F-RS converter developed in our laboratory and previously tested in photovoltaic energy conversion [21]. The value of the capacitor must provide a quasi-constant value of V_{C14} throughout the cycle, while offering the possibility of accepting relatively fast variations of the voltage across it. For this reason, in this simulation, the capacitor C is chosen with a low value equal to 2 μF. Finally, to comply with a high power of the studied system, the voltage of the bus HVDC was set at (200–400)V.

Figure 10 shows the electrical diagram, developed under OrCad, of a Flyback F-RS type matching stage inserted between a PV and an HVDC bus. In the simulation diagram are given the values of the parameters. To provide a means for displaying the progress when the effect of the transformer leakage inductance to the transistor parameters M2. Furthermore, the recovery of the stage voltage RS of this converter is also shown. It can be seen that the magnetic coupling has deliberately been chosen at a low value (k = 0.8) that the transformation ratio is m = 20 to comply with the PV panels for increasing the output voltage).

The results of the simulation of the different voltages in the converter, the output of V_{D6}, on the capacitor V_{C14}, and on the switch Vds of the M2 in **Figure 11**. If these transient phenomena are considered negligible, one can idealize these variations of the main current inside F-RS converter as the linear ones. In spite of a converter considered with a low value of the coupling coefficient, which in the general high voltage Flyback converter can also be seen in **Figure 11** that the voltage is the V_{C14} trend across the capacitor C14 is stable throughout the cycle, a value of approximately V_{C14} = 125 V. A positive consequence is that the switching voltage, Vds, does not exceed the damage threshold value of the MOSFET IRF140 chosen for these simulations.

During the time has pulse to M2, we can observe parasitic pseudo oscillations on V_{D6} in **Figure 11**. During the entire duration of this mode, the diode D6 is blocked and, consequently, the secondary stage of the converter is in an open circuit state. With this time in state, at a primary voltage corresponds a secondary voltage proportional to the transformation ratio m, which comes into resonance due to the parasitic capacitance of D6. The influence of the

http://dx.doi.org/10.5772/intechopen.78768

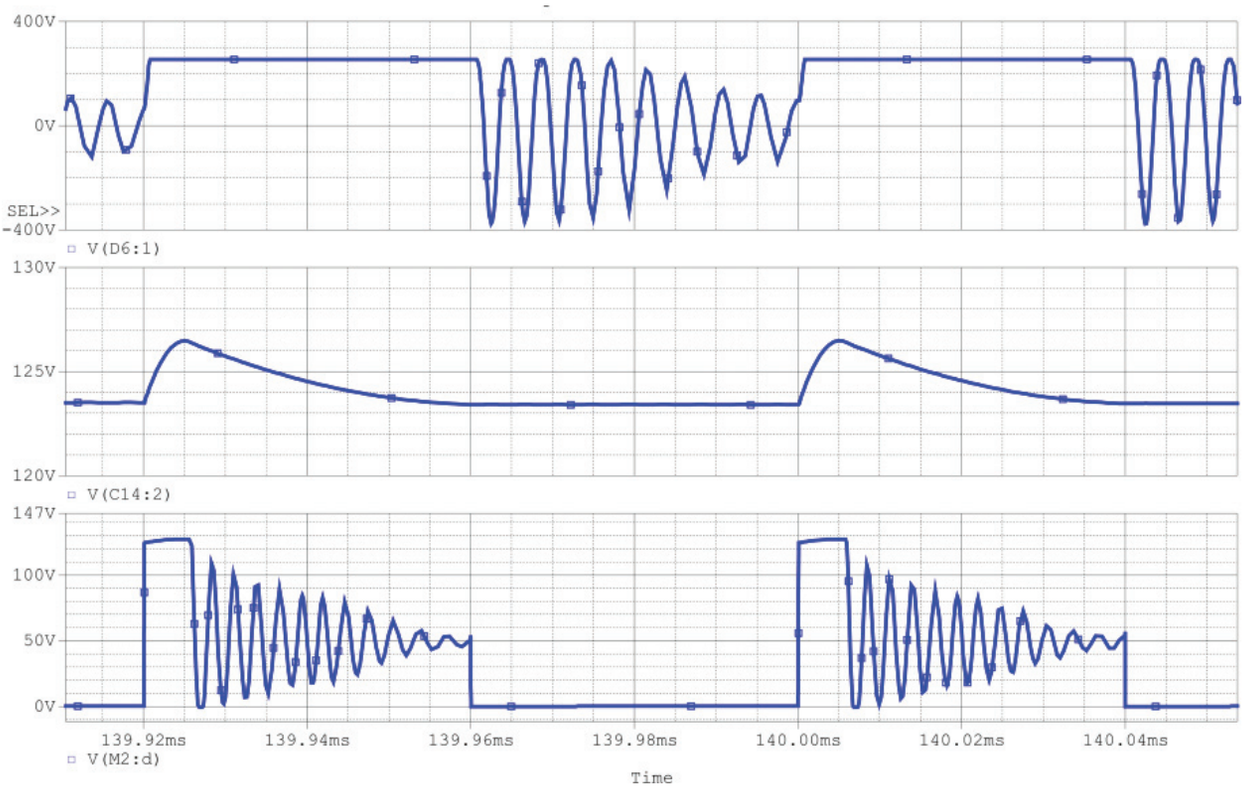


Figure 11. Simulation of the main voltage V_{D6}, V_{C14}, and Vds in the F-RS.

capacitance and values of the coupling coefficient on the shape of the different converter voltages is also highlighted in **Figure 11**. For the selected low value of the intermediate storage capacity, C14 = 2 μF, associated with the small chosen value of the coupling factor k = 0.8, we can observe during all the stopping state (time no pulse) a slight ripple of the voltage V_{C14} around its average value (equal to 125 V in this application). This ripple is due to the transfer of the leakage energy during the turn-off time of the switch. On the other hand, at the beginning of the off state mode of the switch, a transient voltage appears on Vds, followed during the intermediate mode by a huge decrease to zero. Finally (time not pulse), the time main starts with high frequency ripples due to resonance phenomena between the primary inductance and the parasitic capacitances.

Now, we compare the transition from opening to closing at switching time, namely the transition between the two modes, for the basic Flyback and the F-RS converters. We note that during this transition in the Flyback basic system, a very high voltage pulse is applied to the switch. Whereas, in an F-RS, this pulse is immediately transferred via the diode D5 to the recovery capacitor once it reaches a determined threshold value as a function of the capacitor itself, and therefore of V_{C14}, and all other parameters system. As we can see in the above presentation for the fixed experimental parameters selected for this simulation to explain the different modes of the F-RS converter, all these parameters, such as component values, cyclic, transformation ratio and coupling factor, have a huge interdependent influence on the overall behavior of the converter.

4. Conclusion

In this chapter, we presented a specific analysis and calculation leakage inductor in the transformer of individual DC-DC magnetically coupled converters for use in a renewable energy conversion system, including an HVDC bus converter. The DC-DC converter with a high voltage ratio and used upstream, just behind the power source: PV, wind turbine, compressed air storage generator. This solution makes it possible to reduce the voltage Vds applied to the MOSFET transistor. We have shown that in an F-RS converter, even with a low value of the coupling factor, a lower voltage is applied to the transistor which can then be selected from a family of components having a low maximum voltage Vdsmax with a Rdson accordingly low. This choice will increase the performance of the converters. In addition, the energy transfer is improved by a better balance of the service cycle, which is an additional factor of a better efficiency.

Acknowledgements

This work has been funded by Quang Ninh University of Industry, Quang Ninh, Vietnam and Electric power University, Ha noi, Vietnam.

Author details

Nguyen The Vinh[1]* and Vo Thanh Vinh[2]

*Address all correspondence to: dhcnqn@qui.edu.vn

1 Quang Ninh University of Industry, Vietnam

2 Dong Thap University, Vietnam

References

[1] Liang Z, Hung JC, L S, Guo R, Li J, Huang AQ. A high-efficiency pv module-integrated DC/DC converter for pv energy harvest in FREEDM systems. IEEE Transactions on Industrial Electronics. 2011;**26**(3):898-909

[2] Petit P, Zegaoui A, Sawicki JP, Aillerie M, Charles JP. New architecture for high efficiency DC-DC converter dedicated to photovoltaic conversion. Energy Procedia. 2011;**6**:688-694

[3] Petit P. Optimisation du transfert d'énergie dans les systèmes photovoltaïques. thèse, Universitèe de Lorraine. 2011

[4] Wai RJ, Lin CY, Duan RY, Chang YR. High-efficiency power conversion system for kilowatt-level stand-alone generation unit with low input voltage. IEEE Transactions on Industrial Electronics. 2008;**55**(10):3702-3714

[5] Sun J, Sen PC. A general unified large signal model for current programmed DC-to-DC converters. IEEE Transactions on Power Electronics. 1998;**9**(4):414-424

[6] Bidram A, Davoudi A, Balog RS. Control and circuit techniques to mitigate partial shading effects in photovoltaic arrays. IEEE Journal of Photovoltaics. 2012;**2**(4):532-546

[7] Petit P, Aillerie M, Sawicki JP, Charles JP. Push-pull converter for high efficiency photovoltaic conversion. Energy Procedia. 2012;**18**:1583-1592

[8] Petibon S, Alonso C, Estibals B, Seguier L. Multiphase converter structures applied to integrated micro-power application circuits. European Conference on Power Electronics and Applications. 2007;**2007**:1-9

[9] Axelrod B, Berkovich Y, Ioinovici A. Switched coupled-inductor cell for DC-DC converters with very large conversion ratio. In: Proceedings of the Conference of IEEE Industrial Electronics Society; 2006. pp. 2366-2371

[10] Dumrongkittigule V. Tarateeraseth, and W. Khan-Ngern. A new integrated inductor balanced switching technique for common mode EMI reduction in high step-up DC-DC converter. In: Proceedings of the International Zurich Symposium on Electromagnetic Compatibility; 2006. pp. 541-544

[11] Zhao Q, Lee FC. High-efficiency, high step-up DC-DC converters. IEEE Transactions on Power Electronics. 2003;**18**(1):65-73

[12] Park KB, Seong HW, Kim HS, Moon GW, Youn MJ. Integrated boost-sepic converter for high step-up applications. In: Proceedings of the Power Electronics Spec. Conf.; Rohode, Greece; 2008. pp. 944-950

[13] Hariharan S, Schie D. Designing single-switch forward converters. Power Electronics Technology. 2005:38-43

[14] Ryan MJ, Brumsickle WE, Divan DM, Lorenz RD. A new ZVS LCL-resonant push–pull DC–DC converter topology. IEEE Transactions on Industry Applications. 1998;**34**(5):1164-1174

[15] Tomaszuk A, Krupa A. High efficiency high step-up DC/DC converters—A review. Bulletin of the Polish academy of Sciences Technical Sciences. 2011;**59**(4):475-483

[16] Watson R, Lee FC. Utilization of an active-clamp circuit to achieve soft switching in Flyback converters. In: Proc. IEEE Power Electron. Spec. Conf.; 1994. pp. 909-916

[17] Naderian Jahromi A, Faiz J, Mohseni H. A fast method for calculation of transformers leakage reactance using energy technique. Archive of SID. 2003;**16**(1):41-48

[18] William GH, Wilcox DJ. Calculation of leakage inductance in transformer windings. IEEE Transactions on Power Electronics. 1994;**9**(1):121-126

[19] Dauhajre AA. Modelling and estimation of leakage phenomena in magnetic circuit [Thesis]. Pasadena, California: California Institute of Technology. Vol. 22; 1986

[20] Barbosa PM, Barbi I. A single-switch Flyback-current-fed DC–DC converter. IEEE Transactions on Power Electronics. 1998;**13**(3):466-475

[21] Sawicki JP, Petit P, Zegaoui A, Aillerie M, Charles JP. High efficiency step-up hvdc converter for photovoltaic generator. Energy Procedia. 2012;**18**:1593-1600

IntechOpen

IntechOpen